Research Article

NMR IN BIOMEDICINE

Received: 22 February 2010, Revised: 8 July 2010, Accepted: 9 July 2010, Published online in Wiley Online Library: 19 October 2010

(wileyonlinelibrary.com) DOI:10.1002/nbm.1598

High-field MRI of single histological slices using an inductively coupled, self-resonant microcoil: application to *ex vivo* samples of patients with Alzheimer's disease

Rob J. A. Nabuurs[a,b], Ingrid Hegeman[c], Remco Natté[d], Sjoerd G. van Duinen[c,d], Mark A. van Buchem[a], Louise van der Weerd[a,b,e] and Andrew G. Webb[a]*

A simple inductively coupled microcoil has been designed to image tissue samples placed on a microscope slide, samples which can subsequently be stained histologically. As the exact same tissue is used for MRI and histology, the two data sets can be compared without the need for complicated image registration techniques. The design can be integrated into any MRI system using existing commercial hardware. Compared with a commercial 25-mm-diameter birdcage, the signal-to-noise ratio was increased by a factor of 3.8, corresponding to an approximate 15-fold reduction in the data acquisition time. An example is shown of *ex vivo* samples from patients with Alzheimer's disease, in which the coregistration of highly sensitive iron staining and amyloid-β deposits is confirmed. Copyright © 2010 John Wiley & Sons, Ltd.

Keywords: MR microscopy; inductively coupled coils; brain; histology; amyloid-β; Alzheimer's disease; iron staining

INTRODUCTION

MRI is a versatile and powerful tool for the study of many pathological conditions, both *in vivo* and *ex vivo*. In order to verify that changes in MRI signal intensity are a result of pathology, histology remains the gold standard for the determination of the nature of tissue changes. It is highly challenging to coregister precisely the data from histological sections and MRI, primarily because of the deformations and shrinkage that occur when tissue is processed for histology following MR data acquisition. In addition, histological sections would ideally be cut in exactly the same orientation as the acquired MRI data, but, in practice, this is not feasible. To overcome these difficulties, one can develop image processing algorithms to coregister the histological and MRI data by either attempting to correct for three-dimensional deformations or the difference in spatial orientation (1). However, even under the most optimal experimental conditions, the very different spatial resolution of MRI and histological sections makes direct registration a cumbersome task.

To alleviate most of these difficulties and possible errors, a straightforward solution is to obtain MR images directly from the same histological slice that is used for staining. Meadowcroft *et al.* (2) have designed and built a highly specialized coil set-up for horizontal-bore 3-T and 7-T scanners, which enables direct MRI of histological sections, such as those used for standard pathology. The imaged tissue slices were subjected afterwards to several histological stains, thereby showing that it is a worthwhile addition to study and validate MR contrast changes with respect to the pathological substrate, e.g. within brain tissue from Alzheimer's disease (AD). The Meadowcroft coil has excellent sensitivity and performance, but requires relatively specialized expertise to construct and test, and is difficult to implement within the very restricted diameter bore of high-field vertical MR magnets. A simple alternative approach would be to use a small self-resonant microcoil placed around the sample, and to inductively couple this coil to the much larger volume resonator which is provided as standard with the system. The principles of inductively coupling a

* *Correspondence to: A. G. Webb, C. J. Gorter Center for High Field MRI, Department of Radiology, C3-Q, Leiden University Medical Center, Albinusdreef 2, 2333 ZA Leiden, the Netherlands.*
E-mail: a.webb@lumc.nl

a *R. J. A. Nabuurs, M. A. van Buchem, L. van der Weerd, A. G. Webb, M. A. van Buchem, L. van der Weerd, A. G. Webb*
Department of Radiology, C. J. Gorter Center for High Field MRI, Leiden University Medical Center, Leiden, the Netherlands

b *R. J. A. Nabuurs, L. van der Weerd*
Molecular Imaging Laboratories Leiden, MRI Laboratory, Leiden University Medical Center, Leiden, the Netherlands

c *I. Hegeman, S. G. van Duinen*
Department of Neurology, Leiden University Medical Center, Leiden, the Netherlands

d *R. Natté, S. G. van Duinen*
Department of Pathology, Leiden University Medical Center, Leiden, the Netherlands

e *L. van der Weerd*
Department of Anatomy and Embryology, Leiden University Medical Center, Leiden, the Netherlands

Abbreviations used: *AD, Alzheimer's disease; Aβ, amyloid-β; DAB, 3,3′-diaminobenzidine; FOV, field of view; GM, gray matter; NBB, Netherlands Brain Bank; PBS, phosphate-buffered saline; RF, radiofrequency; SNR, signal-to-noise ratio; WM, white matter.*

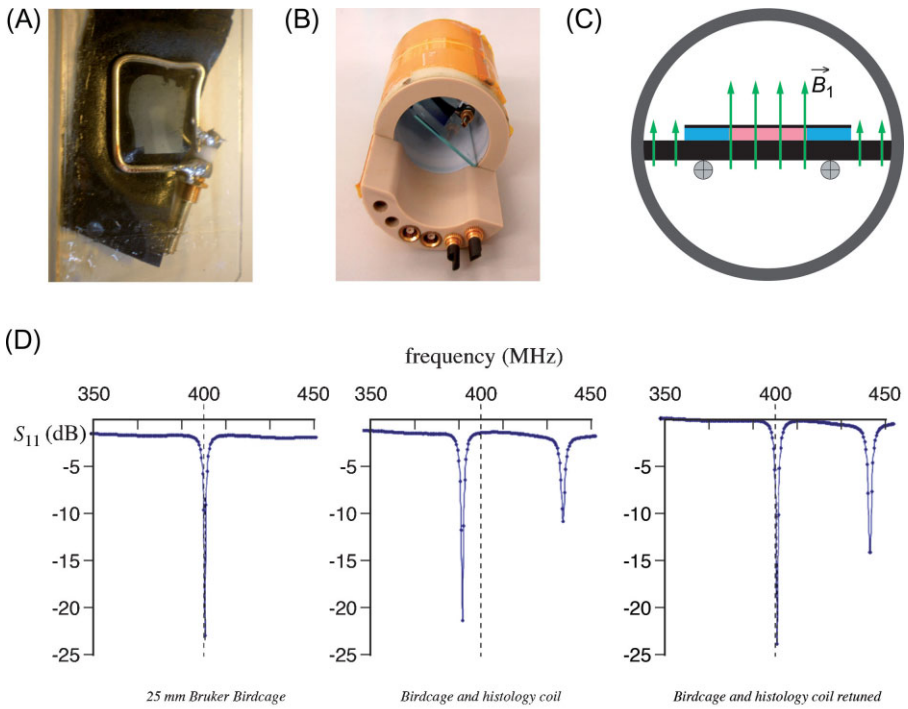

Figure 1. The self-resonant coil is taped onto the back of a standard 25-mm-wide microscope slide, such that it covers a 60-μm-thick brain section, which is mounted on the opposite side in 1 × phosphate-buffered saline (1 × PBS) (A). The slide is positioned in a 25-mm-diameter commercial volume resonator (B), such that it achieves the strongest coupling. Impedance matching of the histology coil is performed using the variable capacitors of the birdcage coil (black screws). A schematic cross-section of the set-up is shown in (C) with the coil on one side of the microscope slide and the sample on the other. The arrows illustrate how the B_1 field is localized as a result of the presence of the inductively coupled coil whilst applying a radiofrequency (RF) pulse via the volume resonator. (D) Network analyzer S_{11} plots from the commercial resonator alone (left), with the strongly coupled coil (center) and after retuning and impedance matched to 50 Ω at 400 MHz (right).

larger transmit coil to a smaller self-resonant 'microcoil' have been covered in many publications, with recent comprehensive signal-to-noise ratio (SNR) analyses in articles by Bilgen (3) and Utz and Monazami (4). These analyses show that the loss in sensitivity using an inductively coupled arrangement, relative to using a microcoil alone, is, at most, a few percent. The approach of using inductively coupled, self-resonant coils for MR microscopy was first shown by Banson *et al.* (5), with the approach having been extended by Glover *et al.* (6) to show coregistered optical and MR images of epidermal cells of *Allium cepa*.

In this study, we have designed and characterized an inductively coupled 'histology coil' for a 9.4-T vertical magnet. The coil is placed at the back of a standard microscope slide so that it completely covers a 60-μm-thick tissue sample. Using these easily produced and replaceable coils, high-resolution images of histological samples can be acquired with an approximate 15-fold reduction in data acquisition time compared with the use of a commercial resonator. After MRI, the same sample underwent staining. In this case, the samples were from *ex vivo* human brain tissue from an ongoing AD study. After MRI scanning, double staining was performed using a new, modified Perls' 3,3′-diaminobenzidine (DAB) stain, combined with immunofluorescence for amyloid-β (Aβ).

MATERIALS AND METHODS

Radiofrequency (RF) coil design

The RF coil was constructed from pure silver 18 AWG wire, shaped into a square with dimensions of 15 × 15 mm^2, approximately 20% larger than the histological slices, so that areas of inhomogeneous B_1 field very close to the wires do not cover the sample (Fig. 1A). For maximum SNR, the microcoil should be strongly coupled to the outer birdcage coil. If the microcoil is tuned to 400 MHz, this introduces a frequency shift that cannot be compensated for by re-adjusting the impedance-matching capacitors of the birdcage. Therefore, the microcoil should be self-resonant at a frequency slightly different from 400 MHz. As outlined by Bilgen (3), one can minimize the current in the larger coil by resonating the microcoil at a slightly lower frequency than that of the larger coil, and then using the lower of the two split resonances. A 1–3.5-pF nonmagnetic variable capacitor (Johansson, Boonton, NY, USA), with a DC breakdown voltage of 1 kV, was used to tune the microcoil to the resonant frequency of approximately 396 MHz. The coil was placed directly onto the back of a microscope slide on which the sample had already been placed (Fig. 1A). Next, the slide was placed in a 25-mm standard Bruker Biospin (Rheinstetten, Germany) high-pass birdcage resonator (Fig. 1B, C), which was connected to a network analyzer (Agilent Technologies, Santa Clara, CA, USA). The orientation of the slide was adjusted to produce the strongest coupling. The mutual inductance splits the resonance frequency into two separate peaks. The low-frequency resonance was impedance matched to 50 Ω at 400 MHz by adjusting the variable capacitors of the birdcage coil (Fig. 1B, D).

Sample preparation

Tissue was obtained from the Netherlands Brain Bank (NBB), Netherlands Institute for Neuroscience, Amsterdam. All material

was collected from donors from whom written informed consent for brain autopsy and the use of the material and clinical information for research purposes had been obtained by NBB. A $12 \times 12 \times 10\text{-mm}^3$ formalin-fixed human brain tissue sample was resected from the neocortex and cut into 60-μm-thick sections with a vibratome (Leica VT 1000 S, Leica Microsystems GmbH, Wetzlar, Germany), followed by immersion in 1 × phosphate-buffered saline (PBS) for at least 24 h to wash out any residual formalin. The tissue section was mounted on a histology slide and a drop of PBS (which had previously been placed under vacuum to reduce air bubbles) was applied to the sample to prevent dehydration. Extreme care was taken to avoid the inclusion of any air bubbles by slowly lowering the coverslip, and the section was sealed with nail polish.

MRI data acquisition

All MRI measurements were conducted on a vertical bore 9.4-T Bruker Avance 400 WB spectrometer, with a 1-T/m actively shielded gradient insert, equipped with ParaVision 5.0 software running with Topspin 2.0. Pulse width calibrations were performed with a 1-ms hermite pulse. The B_1 field homogeneity of the histology coil was evaluated using the double-angle method as described by Stollberger and Wach (7), in which two spin-echo images were acquired with flip angles of 30° and 60°, TR = 4000 ms, TE = 6.5 ms, four signal averages, field of view (FOV) of $16 \times 16\ \text{mm}^2$ and matrix size of 64×64 complex data points.

Imaging experiments were performed using both gradient- and spin-echo sequences. For all sequences, a slice selection pulse was applied to excite a thickness of 2 mm. Scout gradient-echo images were acquired in 1.36 min with FOV = $50 \times 50\ \text{mm}^2$, flip angle of 25°, TR/TE = 75/3 ms, matrix of 128×128 and 10 signal averages. Multiple gradient-echo images were acquired with a flip angle of 22.5°, TR/TE = 75/5–12–19 ms, FOV = $16 \times 16\ \text{mm}^2$, matrix of 256×256 and 200 signal averages, resulting in a 1-h scan with an in-plane resolution of $62 \times 62\ \mu\text{m}^2$. Multiple spin-echo images were obtained in order to calculate T_2 maps, with TR/TE = 2500/10–20–30–40 ms, FOV = $16 \times 16\ \text{mm}^2$, matrix of 128×128 and four averages, obtained in 21 min with a resolution of $125 \times 125\ \mu\text{m}^2$.

Studies of brain tissue of patients with AD

Several previous studies have shown that the pathological hallmarks of AD, namely Aβ plaques and associated iron deposition, can be detected by MR microscopy (8,9). In the current study, brain samples from the entorhinal cortex of a patient with confirmed AD were prepared. Multiple gradient-echo images were acquired with a flip angle of 22.5°, TR/TE = 75/15–25–35–45 ms, FOV = $16 \times 16\ \text{mm}^2$, matrix of 400 × 400 and 200 averages, resulting in a scan time of 1 h 40 min with an in-plane resolution of $40 \times 40\ \mu\text{m}^2$.

Histological staining

Following MR, the same 60-μm section was double stained using a new, modified, highly specific Perls' DAB stain for iron, followed by immunofluorescence Aβ staining. First, the free floating section was immersed for 30 min in 100 mL of methanol with 1 mL 30% H_2O_2, and rinsed subsequently with 96% and 70% ethanol in 1 × PBS to block endogenous peroxidase. A pretreatment similar to that described by LeVine (10,11) was applied at room temperature via 30 min of immersion in 1% $NaBH_4$ in PBS, followed by 20 min in a mixture of 150 μL proteinase K (Sigma-Aldrich Chemie GmbH, Steinheim, Germany), 50 μL Triton-X 100 and 50 mL PBS. After each step, the section was rinsed briefly in 1 × PBS before being placed overnight at room temperature in a solution of 7% potassium-hexacyanoferrate(II)-trihydrate and 3% HCl according to Smith *et al.* (12). Following rinsing in aquadest and 1 × PBS, the section was immersed in 100 mL 0.075% DAB (Sigma) with 50 μL 30% H_2O_2 in 1 × PBS for 10 min, after which the reaction was stopped in aquadest.

Next, the same section was immunostained for Aβ using a standard commercial monoclonal antibody immunostaining method (6F/3D, DakoCytomation, Glostrup, Denmark). One hour of immersion in 85% formic acid and 30 min in trypsin (Type II-S, Sigma), with rinsing with aquadest and 1 × PBS in between, was followed by overnight staining in 1 mL of a 1 : 10 dilution of Aβ antibody at room temperature. Secondary antibody staining consisted of 2 h of immersion with 1 : 100 goat–antimouse–Alexa594 (Invitrogen, Molecular Probes, Breda, the Netherlands) for fluorescence microscopy.

Coregistration and image analysis

Histological images were acquired using a Leica DM/RB microscope equipped with a DFC-420c CCD camera and Leica LAC software. For immunofluorescence, images were acquired in a similar fashion with a XBO xenon lamp and Texas Red filterblock N2.1. All subsequent images were taken with either a 5× or 10× objective lens, allowing automatic photomerging with Adobe Photoshop CS2 to reconstruct a larger image field. A single image was formed from the MR data by summation of all the individual echoes of the multiple gradient-echo sequence. Finally, MR and histological data were coregistered based on the matching of the section outlines and structural features.

RESULTS

RF coil characterization

The frequency shift when the microcoil was placed in the birdcage coil, oriented for maximum coupling, was approximately 10 MHz, as shown in Fig. 1D, with a very small change in the impedance match. The birdcage coil was retuned to 400 MHz using the standard variable impedance-matching capacitors, and the resulting Q value of the retuned coil was almost identical to that of the birdcage alone. Pulse width calibrations for the 25-mm-diameter volume resonator with and without the coupled microcoil showed a decrease of 12 dB in power needed for a 90° pulse when using the inductively coupled coil (Fig. 2A). The SNR was calculated using the MR image shown in Fig. 2B, with a measured SNR increase of a factor of 3.8 when using the coupled system, which corresponds to a reduction in the imaging time by a factor of almost 15. The factor of 3.8 is very close to the expected factor of 4 based on the relative 90° pulse widths. The image in Fig. 2B also demonstrates how the B_1 field is localized when using inductively coupled coils, thereby following the concept shown in Fig. 1C. Although PBS surrounding the brain sample is still seen beyond the edges of the coupled coil in the image acquired solely with the volume resonator, this signal is not picked up when using the coupled coil because of localization of the B_1 field (Fig. 2B, C).

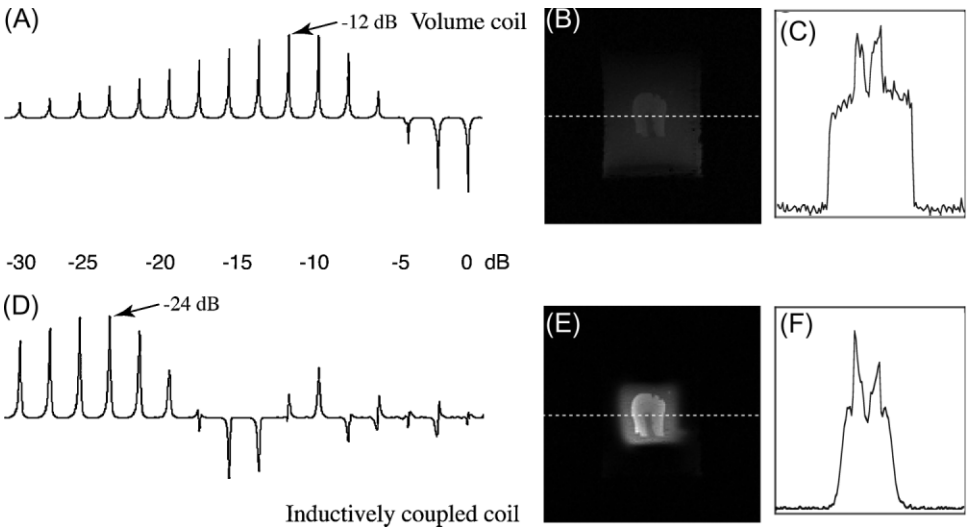

Figure 2. Pulse width calibrations (on logarithmic scale) for the commercial resonator alone (A) and with the coupled histology coil (D) showing a 12-dB reduction in power. Identical scout images obtained from a 60-μm brain section, with the corresponding profile through the horizontal center of the volume resonator, without (B, C) and with (E, F) the histology coil. In addition to illustrating the focused B_1 field, note the decreased noise in (F) compared with (C).

The experimentally measured B_1 field map shows that excitation is homogeneous within the strongly coupled coil (Fig. 3). The homogeneity measured over a FOV of 80% of each of the linear dimensions of the coil showed a standard deviation of approximately 5% in the B_1 field. Similar to a standard surface coil, this homogeneity quickly drops off at the edges of the coil. The excellent homogeneity produced by the coupled coil makes it possible to obtain accurate quantitative maps of relaxation parameters, such as T_2.

Initial scans to compare the performance of the volume coil *vs* the coupled system clearly illustrate the gain in SNR when similar scans were obtained. Standard gradient-echo images (Fig. 4) acquired with the coupled coil show features that are not distinguishable using the volume coil alone. In addition to clearly distinguishable areas of gray (GM) and white (WM) matter, smaller structures within GM are also visible. Similar results were obtained when using a standard multiple spin-echo sequence at a slightly lower resolution (Fig. 5). In addition to increased SNR and image quality, the use of the coupled coil allowed the calculation of more accurate T_2 and T_2^* maps for obtaining quantitative measurements (Figs. Fig.44B, Fig.55B).

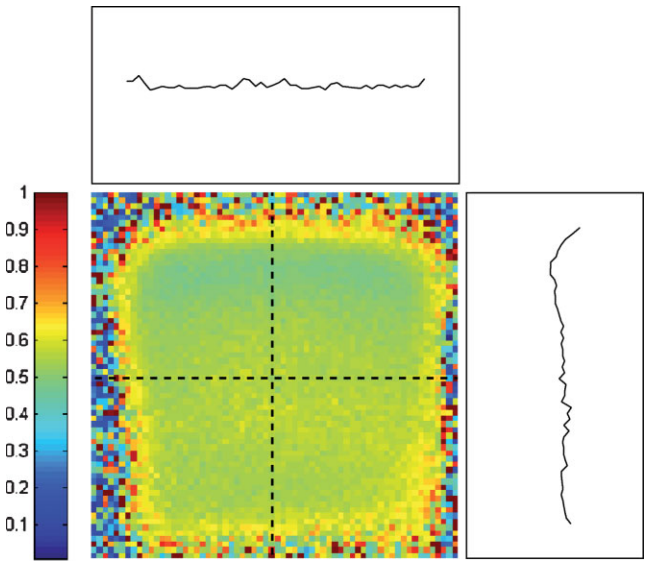

Figure 3. B_1 field map of a 60-μm-thick brain section. Profiles through the horizontal and vertical center demonstrate the uniformity of the coil within the imaging region.

Application to ex vivo human AD tissue

Previously, it has been suggested that, in human AD, brain tissue deposits of Aβ, either colocalized with iron or in the absence of any iron, can create hypointense foci on T_2^*-weighted sequences (2,8,9,13). If the spatial resolution of MRI is sufficiently high, this allows direct correlation with histology. Figure 6 shows a T_2^*-weighted MR image of a tissue section from the entorhinal cortex of a patient with AD, and its corresponding histological images double stained with a modified Perls' stain for iron and with immunofluorescence staining for Aβ. Registration was simply performed based on the section's outline and structural features: the WM vasculature, in particular, could easily be correlated in both image modalities because of the high resolution and SNR of MRI. When examining the complete section, WM and GM are clearly distinguishable in both modalities, in agreement with previous work (2,9), which ascribed the decreased WM signal intensity to an increased iron content of oligodendrocytes and myelin sheets within WM, as confirmed by our modified Perls' staining. Within the MR image, GM shows many small hypointense foci. A similar distribution of dark-brown patches in iron staining indicates regions of high focal iron content (Fig. 6A, B). Furthermore, the diffuse brown background coloration within GM on iron staining shows a similar distribution to the reduced signal intensity on the MR image.

In order to allow a more detailed evaluation and direct correlation between the findings on MR and histology, images were zoomed on a selected region outlined by the box (broken line) (Fig. 6C–E). As depicted by the yellow arrows, many of the MR hypointense foci indeed represent a one-to-one coregistra-

NMR IN BIOMEDICINE

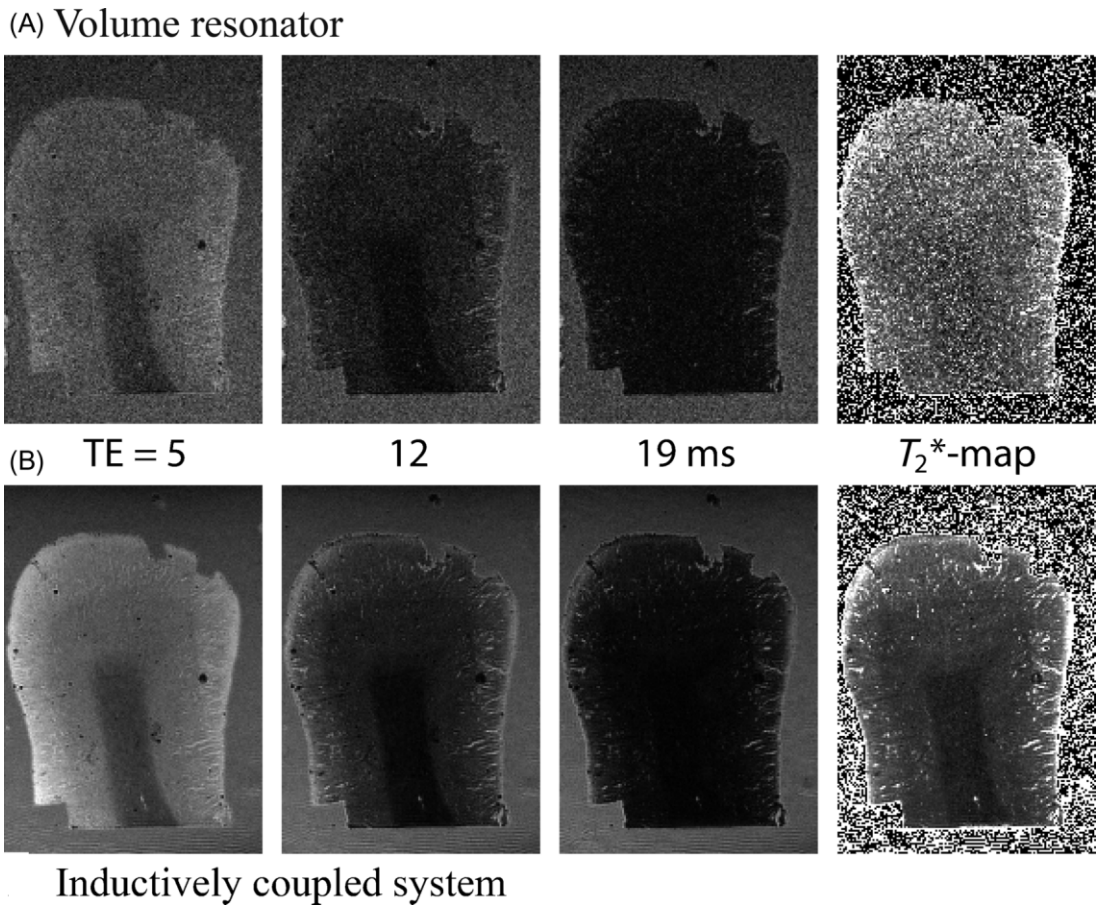

Figure 4. Multiple gradient-echo images and the corresponding T_2^* map from a 60-μm-thick brain section obtained with the volume resonator without (A) and with (B) the inductively coupled histology coil.

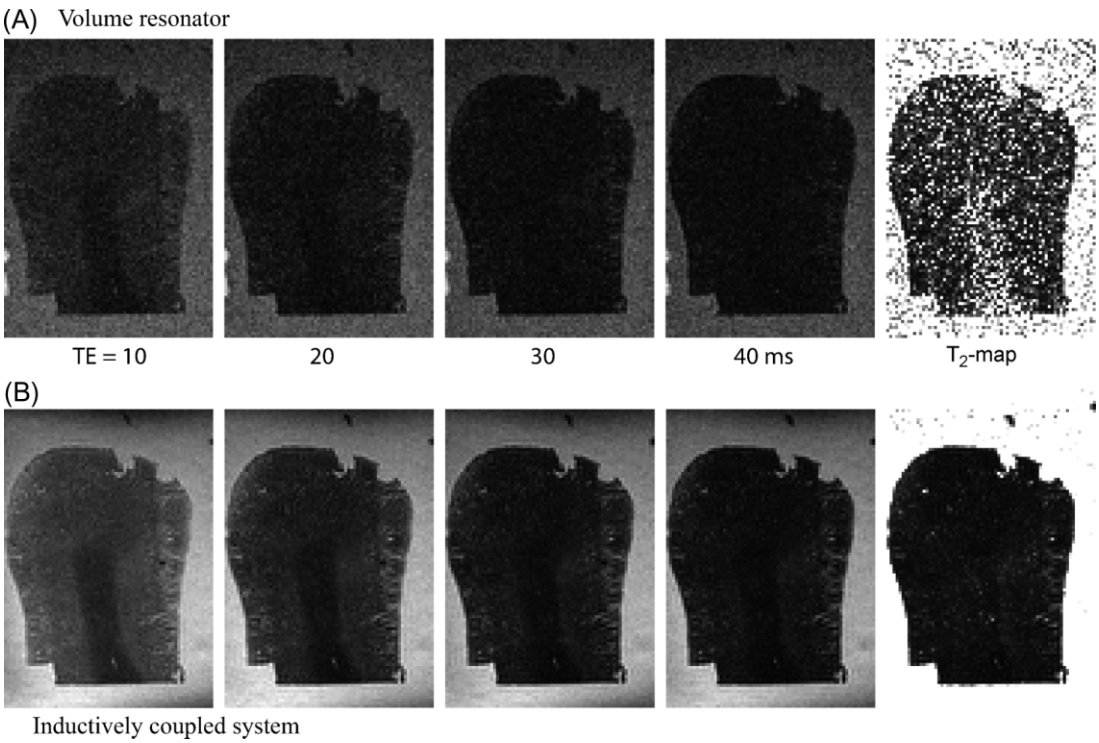

Figure 5. Multiple spin-echo images and the corresponding T_2 map from a 60-μm-thick brain section obtained with the volume resonator without (A) and with (B) the inductively coupled histology coil.

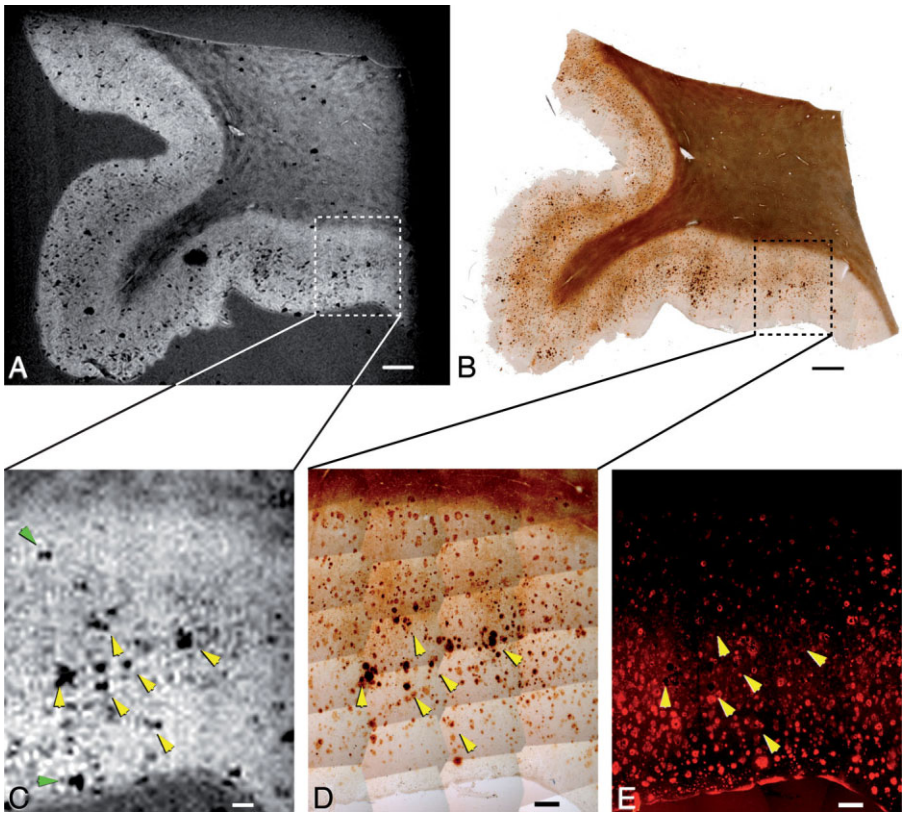

Figure 6. (A) T_2^*-weighted image of a 60-μm brain section of the entorhinal cortex of a patient with known Alzheimer's disease. (B) Microscopy image of the same section after the new, modified Perls' 3,3′-diaminobenzidine (DAB) staining for iron. Dark regions indicate higher iron concentration. For more detailed comparison, a selected region was enlarged, as outlined by the boxes (broken lines), showing the T_2^*-weighted MR image (C), iron staining (D) and amyloid-β (Aβ) immunostaining (E) of the same section. Many hypointense spots within the MR images clearly coregister with focal iron accumulations (yellow arrows), which further colocalize with Aβ as seen in (E). However, not all hypointensities could be coregistered with histological staining (green arrows), and might also be caused by image artifacts, such as tiny air bubbles. Scale bars represent 1000 μm in (A, B) and 200 μm in (C–E).

tion with the dark-brown areas of high focal iron content. However, for distinct areas marked by a more diffuse brown color, suggesting a lower iron concentration, a clear direct correlation could not be made.

When examined carefully, immunostaining for Aβ showed a high Aβ content throughout GM, with almost all deposits correlating with some degree of DAB enhancement of Perls' staining (Fig. 6E). However, although most areas showing an increased iron content were surrounded or covered by Aβ, several small roundish foci did not correlate with Aβ. According to their location and size, these might be iron-loaded microglial cells. Not all MR hypointensities could be correlated directly with either staining (Fig. 6, green arrows), suggesting that another source was responsible for creating these contrast changes. As some of these hypointensities can also be seen outside the tissue section, this suggests that they are likely to be caused by either small impurities or tiny air bubbles.

DISCUSSION

The results presented here indicate that inductively coupled microcoils provide a simple and robust method to acquire high-quality MR images of a single histological section in a reasonable data acquisition time. This offers an alternative approach for the study of various pathological conditions with MR microscopy, allowing contrast changes to be easily validated by direct correlation with histology.

Compared with other approaches, these coils are easy to produce, and also to replace if needed. Made to fit around a histological section of any shape, they are broadly applicable to both horizontal and vertical bore systems, and can be impedance matched up to frequencies well over 1 GHz. Positioned on the back of a microscope slide, the thickness of the histological section can be varied without the need for additional hardware changes. The high-resolution images obtained in this study show sufficiently high SNR, such that slices thinner than the current 60 μm should be possible to image, with even better potential correlation with standard histology.

In this study, formalin-fixed samples were cut using a vibratome and immersed in PBS for several hours prior to imaging, rather than cryosectioning frozen tissue as performed previously (9). The formalin fixation procedure is known to change the MR parameters, but these are partly reversible by PBS immersion. Any extra steps in the slice preparation protocol could lead to additional differences with the *in vivo* situation, and should therefore best be avoided (9,14,15).

The debate about the exact origin of MRI contrast of amyloid plaques is ongoing, but recent work by Meadowcroft *et al.* (9) has shown that both dense amyloid accumulations and iron deposits appear to play a role. Within human AD material, they showed that focal iron load in amyloid plaques registered well with

increased transverse relaxation rates. In contrast, in their mouse model, similar effects were seen even in plaques lacking significant iron accumulation, suggesting that the interaction of water with the highly compacted amyloid fibril masses may be a possible cause of the increased relaxation rates. However, they also showed that standard Perls' DAB staining is not sufficiently sensitive to the levels of iron present, whereas the modified protocol was able to show minute amounts of iron even in some of these murine plaques. On application of these modified protocols to 60-μm, formalin-fixed, human tissue, however, high unspecific background staining hampered clear interpretation, as observed by Meadowcroft *et al.* (9) and in our own studies (data not shown). As we were unable to exploit the more sensitive iron staining in human material, several questions remained unanswered: for example, whether diffuse plaques have any effect on MRI contrast as a result of either iron or Aβ deposits. Therefore, several adjustments were made to the previously published modified Perls' DAB staining protocol to focus on iron accumulation within Aβ deposits of AD brain tissue (11,12). To decrease noniron-specific DAB enhancement, endogenous peroxidase was blocked using methanol before applying the pretreatment described by LeVine (11). The Prussian blue reaction, involving the binding of iron(II) containing ferrocyanide to iron(III) within the tissue, was employed using the concentrations described in Smith *et al.* (12). Next, the peroxidase-like, H_2O_2-dependent oxidation of DAB, used to enhance iron staining, was performed in PBS rather than in aquadest (16). In our experiment, DAB enhancement was optimal when applied for 2 min. The application of the new, modified Perls' DAB staining method to AD brain tissue resulted in similar iron plaque-like structures to those described previously by LeVine (11), and the low unspecific background staining allowed a more accurate registration with MR than described previously using modified Perls' staining. In addition to the high focal iron deposition, many local iron accumulations, which had previously remained undetected, emerged from the background (Fig. 6C). More diffuse iron staining, observed in a sublayer of the cortex, could also be detected on the corresponding MR image, in agreement with recent findings by Duyn *et al.* (17) *in vivo*. This global iron distribution should not be mistaken for unspecific background staining; in this case, the entire cortex would be stained, and the MRI findings would not correspond.

Although this modified staining technique improves the ability to correlate MR signal changes to focal and diffuse iron concentrations, it has a major disadvantage, in that staining for amyloid by standard Thioflavin T or S is not possible, probably because of the very dark pigmentation of the iron-stained sample. As Thioflavin T or S is an indicator of amyloid (as opposed to Aβ), a correlation between the localization of iron and amyloid is not possible. The immunofluorescence stain detects the presence of Aβ, but without the ability to discriminate between dense core amyloid and diffuse plaques containing only fibrillar Aβ. Therefore, using our method, we obtain much higher iron staining efficiency, but, as a consequence, cannot draw any conclusions with regard to whether the MR hypointensities correspond only to iron colocalized with a specific type of Aβ deposition and/or amyloid. Nevertheless, we can conclude that almost all Aβ deposits, whether diffuse plaques or amyloid, contain traces of iron detected by our modified staining method, confirming the results of Meadowcroft *et al.* in human *ex vivo* brain (Fig. 6).

Acknowledgements

The authors acknowledge Frans Prins and Peter Neeskens for their assistance with the microscope and vibratome.

REFERENCES

1. Breen MS, Lazebnik RS, Wilson DL. Three-dimensional registration of magnetic resonance image data to histological sections with model-based evaluation. Ann. Biomed. Eng. 2005; 33: 1100–1112.
2. Meadowcroft MD, Zhang S, Liu W, Park BS, Connor JR, Collins CM, Smith MB, Yang QX. Direct magnetic resonance imaging of histological tissue samples at 3.0T. Magn. Reson. Med. 2007; 57: 835–841.
3. Bilgen M. Inductively-overcoupled coil design for high resolution magnetic resonance imaging. Biomed. Eng. Online 2006; 5: 3.
4. Utz M, Monazami R. Nuclear magnetic resonance in microfluidic environments using inductively coupled radiofrequency resonators. J. Magn. Reson. 2009; 198: 132–136.
5. Banson ML, Cofer GP, Black R, Johnson GA. A probe for specimen magnetic resonance microscopy. Invest. Radiol. 1992; 27: 157–164.
6. Glover PM, Bowtell RW, Brown GD, Mansfield P. A microscope slide probe for high resolution imaging at 11.7 Tesla. Magn. Reson. Med. 1994; 31: 423–428.
7. Stollberger R, Wach P. Imaging of the active B1 field in vivo. Magn. Reson. Med. 1996; 35: 246–251.
8. Benveniste H, Einstein G, Kim KR, Hulette C, Johnson GA. Detection of neuritic plaques in Alzheimer's disease by magnetic resonance microscopy. Proc. Natl. Acad. Sci. USA, 1999; 96: 14,079–14,084.
9. Meadowcroft MD, Connor JR, Smith MB, Yang QX. MRI and histological analysis of beta-amyloid plaques in both human Alzheimer's disease and APP/PS1 transgenic mice. J. Magn. Reson. Imaging, 2009; 29: 997–1007.
10. LeVine SM. Oligodendrocytes and myelin sheaths in normal, quaking and shiverer brains are enriched in iron. J. Neurosci. Res. 1991; 29: 413–419.
11. LeVine SM. Iron deposits in multiple sclerosis and Alzheimer's disease brains. Brain Res. 1997; 760: 298–303.
12. Smith MA, Harris PL, Sayre LM, Perry G. Iron accumulation in Alzheimer disease is a source of redox-generated free radicals. Proc. Natl. Acad. Sci. USA, 1997; 94: 9866–9868.
13. van Rooden S, Maat-Schieman ML, Nabuurs RJ, *et al.* Cerebral amyloidosis: postmortem detection with human 7.0-T MR imaging system. Radiology. 2009; 253: 788–796.
14. Pfefferbaum A, Sullivan EV, Adalsteinsson E, Garrick T, Harper C. Postmortem MR imaging of formalin-fixed human brain. Neuroimage, 2004; 21: 1585–1595.
15. Shepherd TM, Thelwall PE, Stanisz GJ, Blackband SJ. Aldehyde fixative solutions alter the water relaxation and diffusion properties of nervous tissue. Magn. Reson. Med. 2009; 62: 26–34.
16. Danielisova V, Gottlieb M, Burda J. Iron deposition after transient forebrain ischemia in rat brain. Neurochem. Res. 2002; 27: 237–242.
17. Duyn JH, van GP, Li TQ, de Zwart JA, Koretsky AP, Fukunaga M. High-field MRI of brain cortical substructure based on signal phase. Proc. Natl. Acad. Sci. USA, 2007; 104: 11,796–11,801.